Assessment of Lamellar Macular Hole and Macular Pseudohole With a Combination of En Face and Radial B-scan Optical Coherence Tomography Imaging

MASAYUKI HIRANO, YUKI MORIZANE, SHUHEI KIMURA, MIO HOSOKAWA, YUSUKE SHIODE, SHINICHIRO DOI, SHINJI TOSHIMA, KOSUKE TAKAHASHI, MIKA HOSOGI, ATSUSHI FUJIWARA, IPPEI TAKASU, TOSHIO OKANOUCHI, MASAYA KAWABATA, AND FUMIO SHIRAGA

• PURPOSE: **To investigate lamellar macular hole (LMH) and macular pseudohole (MPH) using a combination of en face and radial B-scan OCT.**

• DESIGN: **Retrospective observational case series.**

• METHODS: **SETTING: Institutional study. PATIENT POPULATION: En face and radial B-scan OCT images of 63 eyes of 60 patients diagnosed with LMH or MPH based on an international classification were reviewed. OBSERVATION PROCEDURES: Cases were classified using en face images based on the presence/absence of epiretinal membrane (ERM), retinal folds, parafoveal epicenter of contractile ERM (PEC-ERM), and retinal cleavage. We compared the en face imaging–based classification system with the international classification system using radial B-scan images. We quantitatively evaluated visual function and macular morphology. MAIN OUTCOME MEASURES: Characterization of multimodal OCT-based subtypes of LMH and MPH.**

• RESULTS: **All cases showed ERM and were classified into 4 groups. In the first group, which lacked retinal folds and showed significantly lower visual acuity than the other groups, 81% of eyes had degenerative LMH. In the second group, which lacked PEC-ERM and retinal cleavage and showed significantly lower retinal fold depth, all eyes had MPH. The third group, in which 95% of eyes had symmetric tractional LMH, included eyes with retinal cleavage but without PEC-ERM, and this group showed higher circularity of the foveal aperture and cleavage area than the group with both these features, in which all eyes had asymmetric tractional LMH.**

• CONCLUSIONS: **Multimodal OCT enables classification of LMH and MPH based on pathologic conditions. Retinal traction in particular may be useful for determining treatment methods. (Am J Ophthalmol 2018;188:29–40. © 2018 Elsevier Inc. All rights reserved.)**

AJO.com Supplemental Material available at AJO.com.

Accepted for publication Jan 10, 2018.

From the Department of Ophthalmology, Okayama University Graduate School of Medicine, Dentistry and Pharmaceutical Sciences, Okayama, Japan (M.Hirano, Y.M., S.K., M.Hosokawa, Y.S., S.D., S.T., K.T., M.Hosogi, A.F., F.S.); Takasu Eye Clinic, Okayama, Japan (I.T.); Kurashiki Medical Center, Kurashiki, Japan (T.O.); and Department of Architecture and Building Science, Faculty of Engineering, Yokohama National University, Yokohama, Japan (M.K.).

Inquiries to Yuki Morizane, Department of Ophthalmology, Okayama University Graduate School of Medicine, Dentistry and Pharmaceutical Sciences, 2-5-1 Shikata-cho Kita-ku, Okayama City, Okayama 700-8558, Japan; e-mail: moriza-y@okayama-u.ac.jp

GASS AND ALLEN, BASED ON OBSERVATIONS USING biomicroscopy,[1,2] first reported that lamellar macular hole (LMH) and macular pseudohole (MPH) are diseases that present with foveal formation similar to that of a full-thickness macular hole (FTMH). Differential diagnosis of FTMH, LMH, and MPH has become easier with the advent of optical coherence tomography (OCT), but until recently various definitions for LMH and MPH have been proposed, and different studies on LMH and MPH have used divergent criteria for defining these diseases.[3,4] Therefore, both prognostic and interventional data vary from study to study.[5-8]

In 2013, the International Vitreomacular Traction Study Group established definitions of LMH and MPH based on B-scan OCT image findings.[9] However, with the latest advances in OCT, B-scan image findings not included in these definitions have been clarified, such as lamellar hole–associated epiretinal proliferation (LHEP),[4,10,11] the detailed morphology and changes over time of the ellipsoid zone, and intraretinal splitting.[12,13] Additionally, the morphologic characteristics of LMH differ depending on background pathologies such as high myopia,[14,15] and cases have been reported that cannot be clearly classified as either LMH or MPH.[13] Therefore, the B-scan image–based conventional classification system may not be able to fully account for the diversity of these diseases. Furthermore, classifying LMH and MPH based on macular contour from OCT image findings alone is not sufficient to determine treatment methods; rather, it is essential to classify these conditions by taking into consideration the pathology of each disease.

Govetto and associates[12] recently proposed to divide LMH into tractional and degenerative types. These classifications consider not only the B-scan image morphology but also the LMH pathology, especially the involvement

0002-9394/$36.00
https://doi.org/10.1016/j.ajo.2018.01.016

of retinal traction. These classifications are more practical than the conventional classifications for determining treatment indications, especially with regard to removal of pathologic traction on the retina by vitreous surgery. However, with these classifications, retinal traction is evaluated based on B-scan images alone, and information from a cross-sectional image of the retina is not precise enough to detect retinal traction. Also, information from the cross-sectional image of the retina does not enable detailed evaluation of traction, including traction strength and direction.

One possible method to understand retinal traction in LMH and MPH with a wide observation range is to assess the retina not only with 1 cross-sectional image but also from a coronal view.[16-18] The recent advent of swept-source OCT, which is highly penetrating and has a high scan speed, has made it possible to capture 3-dimensional images of the structure of the retina. In particular, en face images, which are coronal-view images generated after computerized flattening along a specific retinal layer boundary, enable layer-by-layer analysis of retinal folds and deformation of the foveal aperture induced by retinal traction over a wide observation range. Several reports have demonstrated the efficacy of combining en face imaging and B-scan imaging in order to observe LMH and MPH.[10,19,20] However, the research to date has investigated patients with either LMH or MPH, and there has been no investigation that includes a series of patients with both LMH and MPH. Also, previous analyses of en face imaging have not been conducted layer by layer, and these reports have not included quantitative analysis.

In this study, we reassessed LMH and MPH cases that were diagnosed based on the conventional classification system using en face images. We then investigated the relationship between the en face image–based classification system and the conventional classification system using radial B-scan images. Additionally, we quantitatively evaluated visual function, strength of retinal traction, and homogeneity of traction direction for each of the classified groups.

METHODS

• **STUDY DESIGN:** This was a retrospective consecutive observational study.

• **SUBJECTS:** We retrospectively reviewed the charts of a consecutive series of 63 eyes of 60 patients with LMH or MPH who visited Okayama University Hospital, Takasu Eye Clinic, or Kurashiki Medical Center between February 1, 2016 and January 31, 2017. The presence of LMH or MPH was defined according to the definition established by the International Vitreomacular Traction Study Group.[9] Patients with a history of other retinal diseases, such as age-related macular degeneration, diabetic retinopathy, retinal vein occlusion, or uveitis, and those who had received vitreoretinal surgery for any reason were excluded from this study. All of the investigative procedures adhered to the tenets of the Declaration of Helsinki. The study was approved by the Ethics Committee of Okayama University Hospital, Okayama, Japan, and the requirement for informed consent was waived.

• **OPHTHALMIC EXAMINATIONS:** All patients underwent comprehensive ophthalmologic examinations, including best-corrected visual acuity (BCVA) testing with refraction using a 5-m Landolt C acuity chart, indirect and contact lens slit-lamp biomicroscopy, and swept-source OCT (DRI OCT-1 Atlantis; Topcon Corporation, Tokyo Japan). M-charts (Inami, Tokyo, Japan) were used to quantify the degree of metamorphopsia for both vertical and horizontal lines, and the highest score at either line was used for the analysis. Axial length was measured using an optical biometer (OA-2000; Tomey, Nagoya, Japan).

• **RADIAL B-SCAN IMAGING AND EN FACE IMAGING WITH SWEPT-SOURCE OPTICAL COHERENCE TOMOGRAPHY:** Two OCT imaging methods were used in this study: radial B-scan imaging and en face imaging. Radial B-scan imaging included a total of 12 radial scans centered in the fovea, with a scan length of 12 mm at 15-degree intervals. For en face imaging, 3-dimensional OCT volume data of the retina were obtained over a 6 × 6-mm area consisting of 512 × 256 A-scans. To construct en face images, En View version 1.0.1 software (Topcon Corporation) was used, aligning the 3-dimensional OCT volume data along a specific retinal layer boundary to generate an en face image at an arbitrary depth.

• **RADIAL B-SCAN IMAGE ANALYSIS:** Presence/absence of ellipsoid zone disruption and LHEP were detected using radial B-scan imaging.

• **EN FACE IMAGE ANALYSIS:** We performed both qualitative and quantitative analyses of en face images (Figure 1). The qualitative analyses included determining the presence/absence of the following 4 items: epiretinal membrane (ERM), retinal folds, parafoveal epicenter of constriction in the ERM (PEC-ERM), and retinal cleavage. The quantitative analyses included the following 3 items: maximum depth of the retinal folds from the internal limiting membrane (ILM; Supplementary Figure 1, available at AJO.com), area and circularity of the foveal aperture at the ILM level (Supplementary Figure 2, available at AJO.com), and maximum area and circularity of retinal cleavage (Supplementary Figure 2).

Presence of ERM and PEC-ERM were detected using en face images at the ILM level (Figure 1, Top row). To obtain en face images in order to detect ERM and PEC-ERM, we

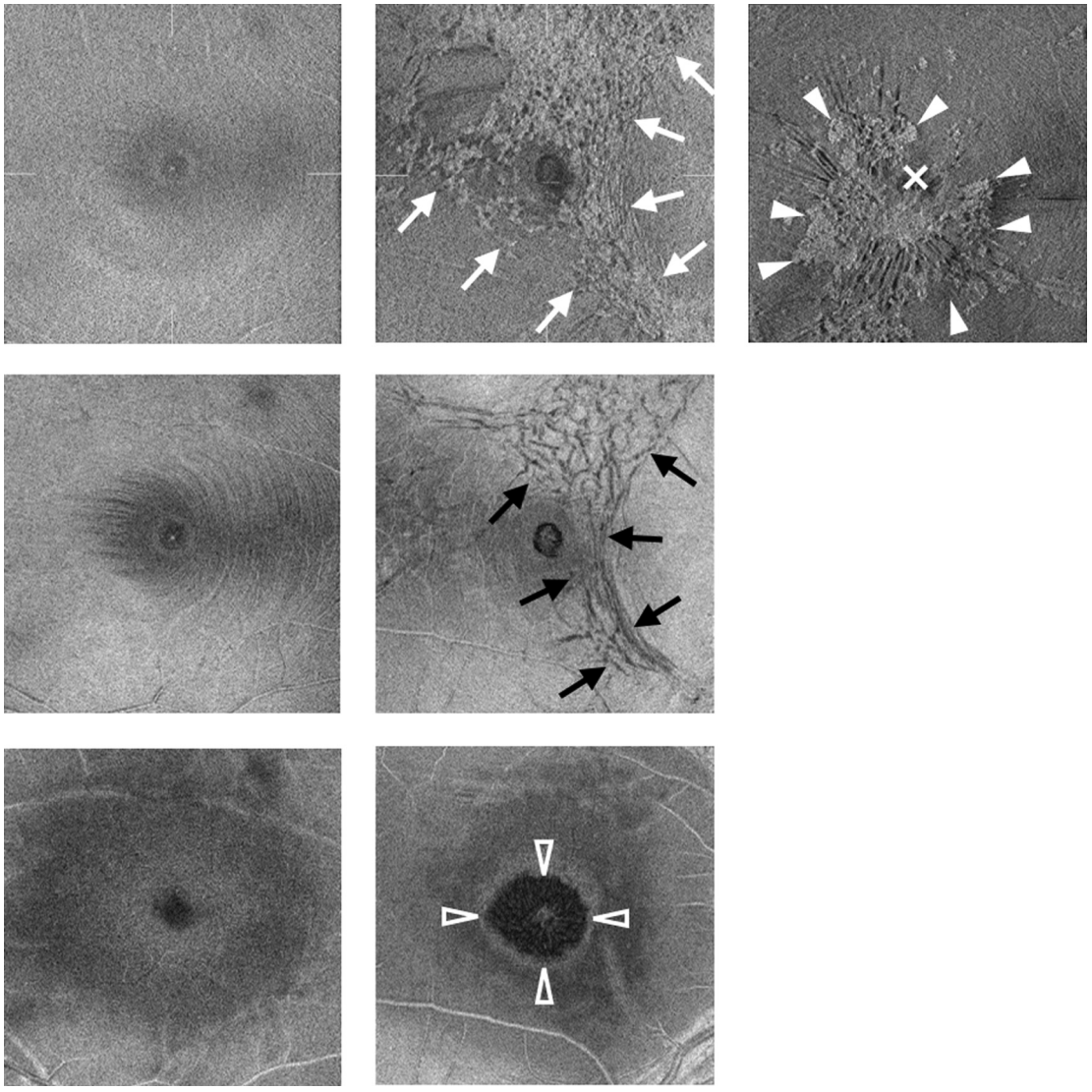

FIGURE 1. Representative en face images of epiretinal membrane (ERM), parafoveal epicenter of contractile ERM (PEC-ERM), retinal folds, and retinal cleavage. (Top left) En face image of a normal eye at the internal limiting membrane (ILM) level shows a smooth surface. (Top middle) ERM at the ILM level (arrows). (Top right) PEC-ERM (arrowheads) and radiating folds owing to ERM contraction. X shows the fovea. (Second left) En face image 10 μm below the ILM in a normal eye. The optic nerve fiber track can be seen, but retinal folds are not observed. (Second right) Retinal folds at 10 μm below the ILM. Retinal folds are observed as black linear structures (arrows). (Bottom left) En face image taken at the outer nuclear layer level in a normal eye. No retinal cleavage can be seen. (Bottom right) Retinal cleavage at the outer nuclear layer level. Retinal cleavage is observed as a well-defined area around the macula (arrowheads).

used the ILM as a reference plane for flattening and a slab thickness of 0 μm. The presence of retinal folds was detected from en face images obtained 10 μm below ILM level (Figure 1, Second row). Similarly, we used the ILM as a reference plane for flattening with a slab thickness of 0 μm to detect retinal folds. To detect retinal cleavage, we obtained en face images using the retinal pigment epithelium as a reference plane for flattening and a slab thickness of 31.2 μm (Figure 1, Bottom row). Under these conditions, the slab was moved up or down in order to determine the depth at which the maximum area of retinal cleavage could be obtained.

The maximum depth of the retinal folds from the ILM level was measured by detecting the slab depth at which the black lines corresponding to the retinal folds disappeared on the en face image (Supplementary Figure 1). Area and circularity of the foveal aperture at the ILM level were measured from en face images using ImageJ version 1.48 software (National Institutes of Health, Bethesda, Maryland, USA) by manually circumscribing the boundary

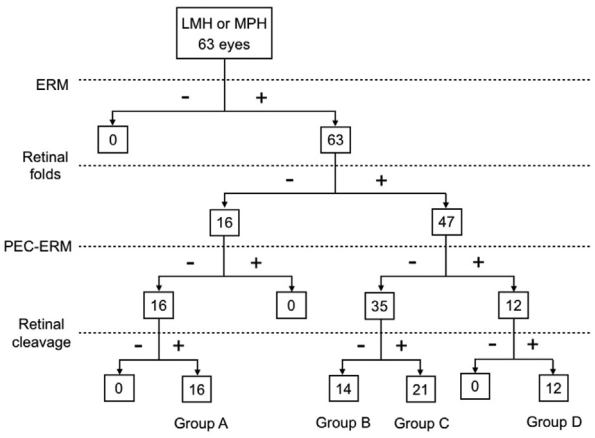

FIGURE 2. Flow chart used to classify lamellar macular hole and macular pseudohole based on en face image findings. ERM = epiretinal membrane; LMH = lamellar macular hole; MPH = macular pseudohole; PEC-ERM = parafoveal epicenter of contractile ERM.

of the foveal aperture region (Supplementary Figure 2). The maximum area and the circularity of the cleavage area were measured using ImageJ by manually circumscribing the boundary of the cleavage area (Supplementary Figure 2). The circularity values range from 0 (infinitely elongated polygon) to 1 (perfect circle).[21] All qualitative analyses were performed by 3 retinal specialists (M. Hirano, Y.M., S.K.).

• **MAIN OUTCOME MEASURES:** The main outcome measures were (1) classification of LMH and MPH using en face imaging, (2) the relationship between an en face image–based classification system and a conventional classification system, and (3) morphologic and functional characterization of the en face image–based classification system.

• **STATISTICS:** BCVAs were recorded as decimal values and converted to logarithm of the minimal angle of resolution (logMAR) units for statistical analysis. Statistical analyses were performed using Statistical Package for the Social Sciences software (SPSS, version 24.0.0.0; IBM Corporation, Armonk, New York, USA). The statistical techniques used for each analysis are described in the results section. A P value of $<.05$ was considered to be statistically significant.

RESULTS

• **LAMELLAR MACULAR HOLE AND MACULAR PSEUDOHOLE CLASSIFICATIONS BASED ON EN FACE IMAGE:** In this study, all cases were classified using the presence or absence of the following en face image–based results: ERM, retinal folds, PEC-ERM, and retinal cleavage. Typical photographs of these findings are shown in Figure 1. ERM was determined by the presence of an irregular membrane-like structure at the height of the ILM within the en face image (Figure 1, Top center). The ERM cases included a case with radiating retinal folds with a contractile epicenter in the parafoveal region (Figure 1, Top right). This case had a particularly localized distribution of retinal traction compared to the other ERM cases, and this result was considered to be characteristic of contractile ERM[19] and was therefore defined as PEC-ERM. Retinal folds were observed as a low-reflection linear structure at a depth of 10 μm from the ILM level (Figure 1, Second right). Retinal cleavage was considered to be a low-reflection region centered around the fovea ranging in level from the outer plexiform layer (OPL) to the outer nuclear layer (ONL) (Figure 1, Bottom right). Figure 2 shows the flow chart used to classify each case using en face image results. Although there were differences in degree of ERM, ERM was present in all cases. Retinal folds were observed in 47 eyes (74%) and were not observed in 16 eyes (26%). PEC-ERM was not seen in any of the 16 cases without retinal folds, but retinal cleavage was observed in all of these cases (Group A). The 47 eyes with observed retinal folds were classified into 3 other groups depending on the presence or absence of PEC-ERM and the presence or absence of retinal cleavage. Fourteen eyes (14/63; 22%) showed retinal folds but lacked PEC-ERM and retinal cleavage and were classified as Group B. Twenty-one eyes (21/63; 33%) showed retinal folds, lacked PEC-ERM, and showed retinal cleavage and were classified as Group C. Finally, 12 eyes (12/63; 19%) showed retinal folds, PEC-ERM, and retinal cleavage and were classified as Group D. All cases that showed both retinal folds and PEC-ERM also showed retinal cleavage. The demographic data for these 4 groups are presented in Table 1. There was no significant difference in age or axial length between the groups. Axial length was equal to or greater than 26 mm in 2 eyes (13%) in Group A, 0 eyes (0%) in Group B, 4 eyes (19%) in Group C, and 2 eyes (17%) in Group D.

• **COMPARISON OF CLASSIFICATION OF LAMELLAR MACULAR HOLE AND MACULAR PSEUDOHOLE BASED ON EN FACE IMAGING WITH CONVENTIONAL CLASSIFICATION BASED ON B-SCAN IMAGING:** We compared the en face image–based classification system (Groups A-D) and the conventional B-scan image–based classification system. The conventional classification system was based on a combination of the definitions proposed by the International Vitreomacular Traction Study Group[9] and Govetto and associates.[12] The presence of MPH was defined according to the following OCT features: invaginated or heaped foveal edges, concomitant ERM with central opening, steep macular contour to the central fovea with near-normal central foveal thickness, and no loss of retinal tissue. The presence of LMH was defined according to

TABLE 1. Patient Characteristics in Each Group Classified Based on En Face Image Results

	Group A N = 16	Group B N = 14	Group C N = 21	Group D N = 12	*P* Value
Age (y)	74.0 ± 9.1	69.3 ± 6.2	70.8 ± 7.5	65.9 ± 12.6	.149
Axial length (mm)	24.7 ± 2.7	23.5 ± 2.5	25.1 ± 2.9	24.7 ± 2.4	.492
Radial B-scan type					
MPH, eyes (%)	0 (0%)	14 (100%)	0 (0%)	See Table 2	NA
Tractional LMH, eyes (%)	3 (19%)	0 (0%)	20 (95%)	See Table 2	NA
Degenerative LMH, eyes (%)	13 (81%)	0 (0%)	1 (5%)	See Table 2	NA
EZ disruption, eyes (%)	11 (69%)	1 (7%)	2 (10%)	0 (0%)	NA
LHEP, eyes (%)	13 (81%)	0 (0%)	1 (5%)	0 (0%)	NA
M-chart score	0.34 ± 0.38	0.34 ± 0.53	0.45 ± 0.52	0.38 ± 0.73	.935
Aperture area at ILM level (mm^2)	0.31 ± 0.16	0.22 ± 0.20	0.21 ± 0.12	0.20 ± 0.12	.202
Maximum cleaved area (mm^2)	0.78 ± 0.39	NA	1.43 ± 0.69	1.60 ± 2.28	.141

EZ = ellipsoid zone; ILM = internal limiting membrane; LHEP = lamellar hole–associated epiretinal proliferation; LMH = lamellar macular hole; MPH = macular pseudohole; NA = not applicable.

Data are presented as mean ± standard deviation unless otherwise indicated.

TABLE 2. Radial B-scan Results for Group D (N = 12)

Radial B-scan Type	PEC-ERM Scan	Orthogonal Scan
MPH, eyes (%)	0 (0%)	2 (17%)
Tractional LMH, eyes (%)	12 (100% asymmetric)	9 (75% symmetric)
Degenerative LMH, eyes (%)	0 (0%)	1 (8%)

LMH = lamellar macular hole; MPH = macular pseudohole; PEC-ERM = parafoveal epicenter of contractile epiretinal membrane.

the following OCT features: presence of irregular foveal contour, separation of the layers of the neurosensory retina, and absence of full-thickness macular defects. Based on the classification system proposed by Govetto and associates,[12] if an LMH showed a sharp-edged schisis-like appearance between the OPL and the ONL, it was classified as "tractional LMH," and if an LMH showed a round-edged cavitation, it was classified as "degenerative LMH." Typical B-scan images for these 3 types are shown in Supplementary Figure 3 (Supplemental Material available at AJO.com). Tables 1 and 2 show the comparison of en face image–based classification results and conventional B-scan classification results. Representative cases from each group are shown in Figure 3, and the data describing all cases for each group are shown in Supplementary Tables 1-4 (Supplemental Material available at AJO.com). In Group A (n = 16), 13 eyes (81%) were classified as degenerative LMH, 3 eyes (19%) were classified as tractional LMH, and no eyes were classified as MPH. In Group B (n = 14), all cases were classified as MPH. In Group C (n = 21), 20 eyes (95%) were classified as tractional LMH, 1 eye (5%) was classified as degenerative LMH, and no eyes were classified as MPH. In Group D (n = 12), all cases were classified as tractional LMH by images of the cross section through the PEC-ERM. However, when images of the cross sections orthogonal to the cross section through the PEC-ERM were used, 9 eyes (75%) in Group D were classified as tractional LMH, 2 eyes (17%) were classified as MPH, and 1 eye (8%) was classified as degenerative LMH (Table 2). When images of the cross section passing through the PEC-ERM were used, the measured retinal thickness was significantly thicker on the side with the PEC-ERM than on the opposite side, leading to a classification of asymmetric LMH (Supplementary Figure 4, available at AJO.com, and Table 2). In contrast, images of the cross sections orthogonal to the cross section through the PEC-ERM led to all cases being classified as symmetric LMH. Ellipsoid zone disruption and LHEP were seen in 69% and 81% of cases in Group A, respectively (Table 1).

• **RELATIONSHIP BETWEEN EN FACE IMAGE–BASED CLASSIFICATION AND VISUAL FUNCTION:** The mean visual acuity of Group A (0.44 ± 0.41) was significantly lower than that of the other groups (0.05 ± 0.11, 0.17 ± 0.18, 0.17 ± 0.22 in Groups B, C, and D, respectively; $P < .001$, 1-way analysis of variance (ANOVA); *P* values of Group A vs B, Group A vs C, and Group A vs D were $P < .001$, $P < .016$, and $P < .046$, respectively, Turkey-Kramer test; Figure 4). No significant difference in visual acuity was seen among Groups B, C, and D. There was no significant difference in the M-chart score among all the groups (Table 1).

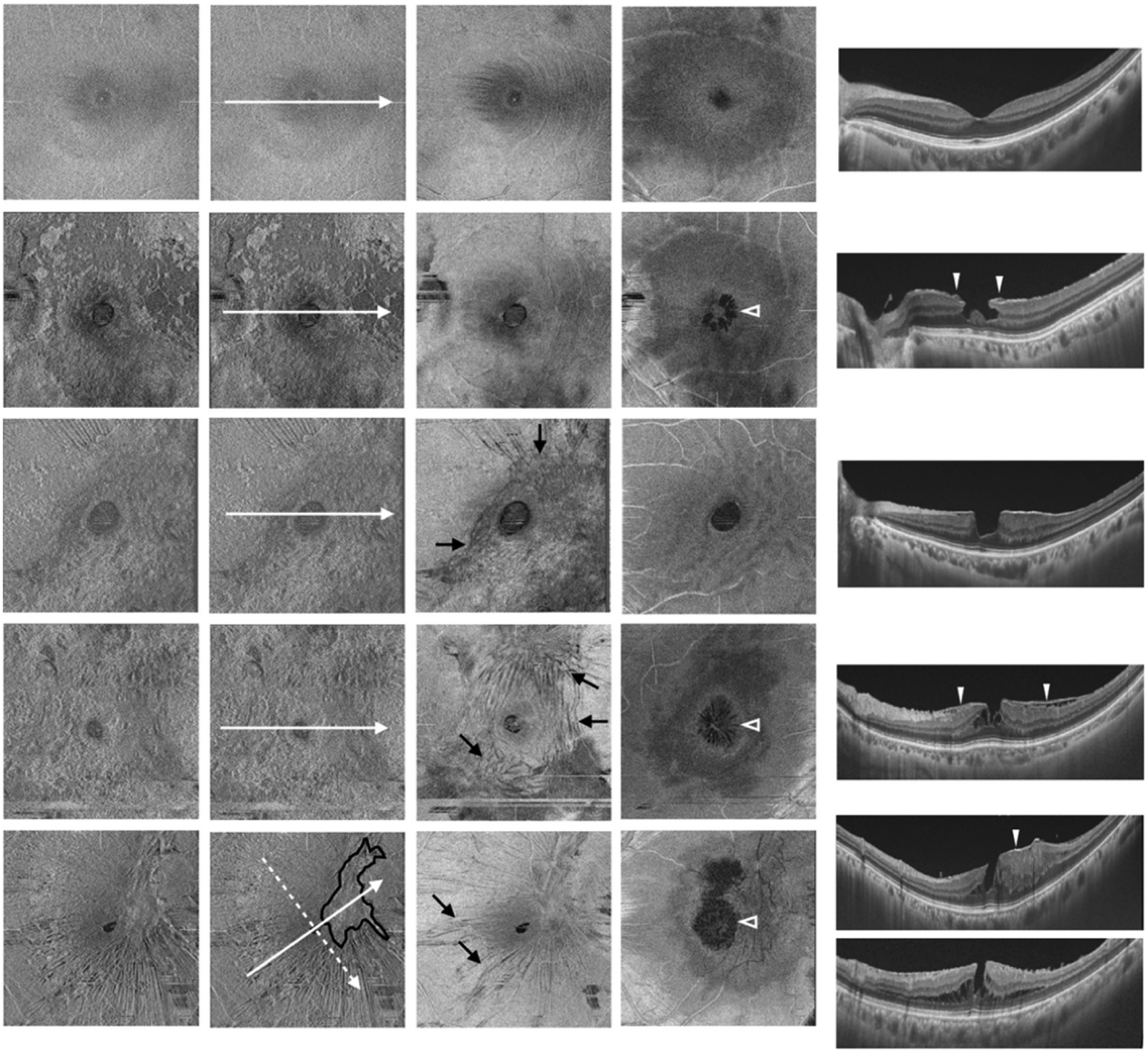

FIGURE 3. Representative en face images at internal limiting membrane (ILM) level (first and second columns), at 10 μm below ILM level (third column), and at approximately the outer nuclear layer level (fourth column), and B-scan images (fifth column). The first row is from a normal subject, and the second to the fifth rows are images of patients from Groups A-D in Figure 2, respectively. The white solid and dotted arrows in the second column indicate the location corresponding to the B-scan section of the fifth column. (Top row) A 53-year-old man without eye disease. Epiretinal membrane (ERM) and retinal folds are not observed in en face image or B-scan image. (Second row) A 70-year-old female patient from Group A. ERM (first column) and retinal cleavage (arrowhead in the fourth column) were seen with en face imaging, but retinal folds were not observed. The B-scan image indicates that this case is degenerative LMH with lamellar hole–associated epiretinal proliferation (arrowheads in the fifth column). (Third row) A 73-year-old female patient from Group B. ERM (first column) and retinal folds (arrows in the third column) were found with en face imaging, but retinal cleavage was not observed. The B-scan image indicates that this case is macular pseudohole (MPH) with ERM (arrowheads in the fifth column). (Fourth row) A 74-year-old female patient from Group C. ERM (first column), retinal folds (arrows in the third column), and retinal cleavage (arrowhead in the fourth column) were found by en face imaging. The B-scan image indicates that this case is symmetric tractional LMH with ERM (arrowheads in the fifth column). (Fifth row) A 47-year-old male patient from Group D. Parafoveal epicenter of contractile ERM (PEC-ERM, outlined in the second column), retinal folds (arrows in the third column), and retinal cleavage (arrowhead in the fourth column) were observed by en face imaging. The B-scan image indicates that this case is asymmetric tractional LMH (fifth column upper) when the cross section (the optical coherence tomography [OCT] scan direction is indicated by solid arrow in the second column) passed through the PEC-ERM (arrowhead in the fifth column upper). The cross-section image (the fifth column lower) vertical to the solid arrow (the OCT scan direction is indicated by dotted arrow in the second column) indicates that this case has not only asymmetric tractional LMH but also symmetric tractional LMH.

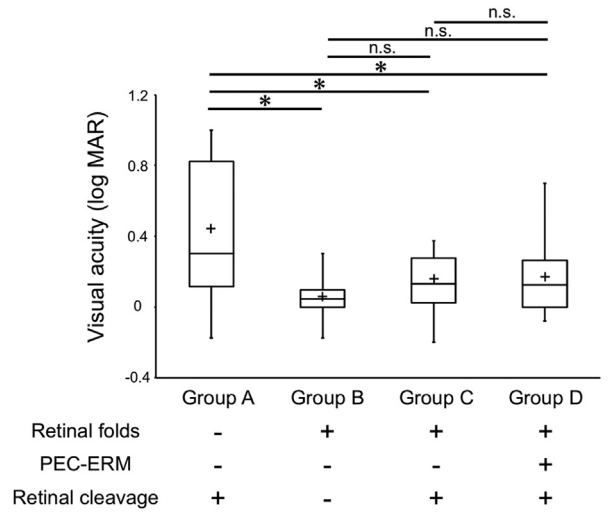

FIGURE 4. Comparison of visual acuity by group. *$P < .05$. logMAR = logarithm of the minimal angle of resolution; n.s. = not significant; PEC-ERM = parafoveal epicenter of contractile epiretinal membrane.

• QUANTITATIVE ANALYSIS OF EN FACE IMAGING: We compared the maximum depths of the retinal folds in Groups B, C, and D (Group A did not contain cases with retinal folds). Groups C (71.5 ± 19.0 μm) and D (77.6 ± 33.1 μm) had significantly deeper folds than Group B (49.4 ± 21.0 μm; $P = .012$, 1-way ANOVA; P values of Group B vs C and Group B vevsrsus D were .042 and .016, respectively, Turkey-Kramer test; Figure 5, Top left). The difference between Groups C and D was not significant.

There was no significant difference in either the foveal aperture area or the maximum retinal cleavage area between groups ($P = .202$ and $P = .141$, respectively, 1-way ANOVA; Table 1). The circularity of the foveal aperture at the ILM level was lowest in Group D, followed by Group C (0.89 ± 0.03, 0.77 ± 0.13, 0.68 ± 0.12 in Groups B, C, and D, respectively; $P < .001$, 1-way ANOVA; P values of Group B vs C, Group B vs D, and Group C vs D were $P = .005$, $P < .001$, and $P = .049$, respectively, Turkey-Kramer test; Figure 5, Top right). Group D had a significantly lower circularity of the maximum retinal cleavage area compared to Group C (0.75 ± 0.14 and 0.64 ± 0.13 in Groups C and D, respectively; $P = .03$, unpaired t test; Figure 5, Bottom).

DISCUSSION

IN THIS STUDY, WE INVESTIGATED CASES WITH LMH OR MPH that were diagnosed based on a conventional international classification using a combination of en face and radial B-scan images. We observed the following important findings on LMH and MPH classifications. First, LMH and MPH diagnosed based on the conventional classification system can be broadly divided into 2 groups based on the presence/absence of retinal folds detected by en face OCT. A total of 81% of the cases in the group without retinal folds (Group A) were classified as "degenerative LMH" by radial B-scan OCT, as defined by Govetto and associates[12] (Figure 3, Table 1). However, the groups with retinal folds (Groups B, C, and D) were more likely to show "tractional LMH" and MPH, as defined by Govetto and associates[12] and the International Vitreomacular Traction Study Group.[9] Second, we observed that the retinal fold (-) group (Group A) had a significantly higher rate of LHEP and ellipsoid zone disruption and lower visual acuity compared to the retinal fold (+) groups (Table 1). Third, the retinal fold (+) groups could be divided into 2 groups based on the presence/absence of retinal cleavage, and cases with retinal cleavage were more likely to show "tractional LMH," as defined by Govetto and associates,[12] while cases without retinal cleavage were more likely to show MPH as defined by the International Vitreomacular Traction Study Group (Figure 3, Table 1).[9] Fourth, although few in number, there were cases that presented with radial B-scan images that did not correspond to classifications of both the first and third results above (Supplementary Tables 1, 3, and 4). These results support the proposal by Govetto and associates[12] that LMH defined by international classification can be further classified into 3 subtypes: tractional LMH, degenerative LMH, and mixed-type LMH. Furthermore, tractional LMH is closer to the pathology of MPH owing to the involvement of retinal traction, as opposed to degenerative LMH, for which retinal traction has very little pathologic involvement. These results support the findings by Gaudric and associates[19] that MPHs with stretched edges (equivalent to tractional LMH in Govetto's classification) are part of the spectrum of MPH and are induced by ERM contraction.

In addition to viewing retinal folds, use of en face OCT also enables visualization of ERM distribution and the presence/absence of a contractive epicenter of ERM (PEC-ERM), making it possible to ascertain the details of retinal traction in MPH and LMH. In particular, the cases that were both retinal fold positive and retinal cleavage positive (considered to be tractional LMH cases) were classified into 2 groups based on ERM distribution. Cases showing diffuse distribution presenting as symmetric retinal cleavage on B-scan imaging were classified as Group C, while cases with localized strong contraction in the parafovea (PEC-ERM) were classified as Group D. The cases in Group D presented with varying morphology depending on scan direction, including both symmetric and asymmetric tractional LMH, MPH, and degenerative LMH (Table 2 and Supplementary Table 4). Recently, Haouchine and associates[3] and Michalewski and associates[22] each reported that cross section images of LMH differ depending on scan direction. Our results not

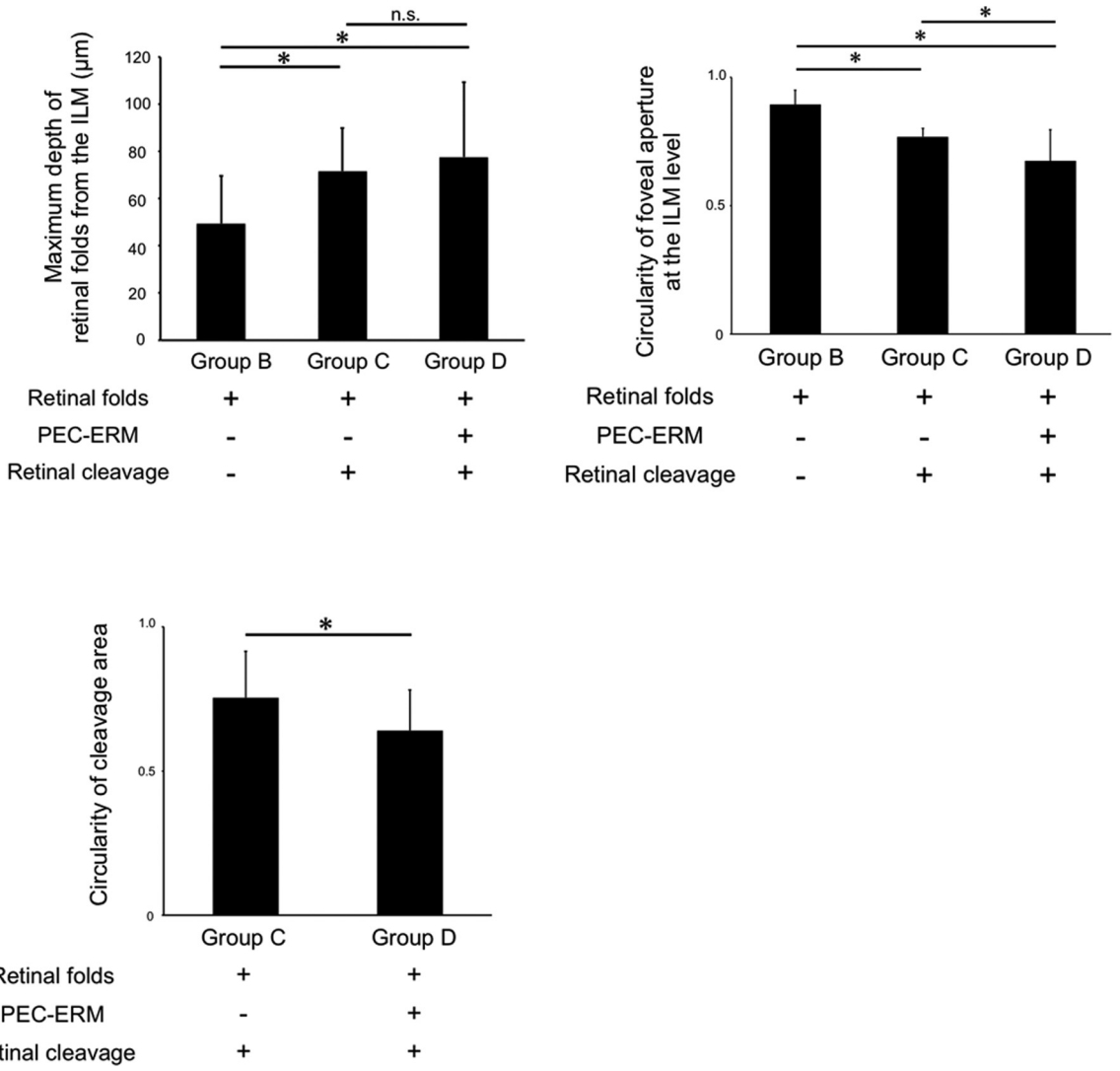

FIGURE 5. Comparisons of the maximum depth of retinal folds and circularities of the foveal aperture at the internal limiting membrane level and retinal cleavage area. *$P < 0.05$. ILM = internal limiting membrane; n.s. = not significant; PEC-ERM = parafoveal epicenter of contractile epiretinal membrane.

only agreed with these reports but also revealed that the positional relationship between PEC-ERM and the scan line is the cause of this phenomenon. Interestingly, in cases with PEC-ERM, the B-scan images obtained from scans that passed through the fovea but not through the PEC-ERM showed schisis-like symmetric cleavages (Figure 6). These schisis-like cleavages were found to broadly expand in an area corresponding to the radiating retinal folds around the PEC-ERM in en face images (Figure 6, Top right). Generally, when folds are generated in a thin elastic membrane, compression stress is exerted in a direction vertical to the direction of the folds (Poisson effect).[23,24] Indeed, as shown in Figure 6, the centripetal force towards the fovea in Group D was exerted on the inner retina, generating a space gap between the outer and inner retina. This may have caused the broad schisis-like retinal cleavage in the area of the radiating retinal folds. Previously, retinal cleavage was thought to have been a result of centrifugal traction on the fovea caused by ERM.[3,9,19,25] However, our results indicate that the traction exerted on the fovea in LMH with PEC-ERM is not simply centrifugal on the entire circumference but is more complicated than conventionally thought. Based on these results, conducting only horizontal and vertical B-scan imaging is insufficient to achieve an accurate classification of LMH and MPH, and it is important to conduct a multimodal OCT assessment using a combination of en face and radial B-scan images.

In this study, we also quantitatively evaluated the strength of retinal traction using the maximum depth of the deepest retinal fold (Supplementary Figure 1 and Figure 5). Further, we evaluated the homogeneity of the

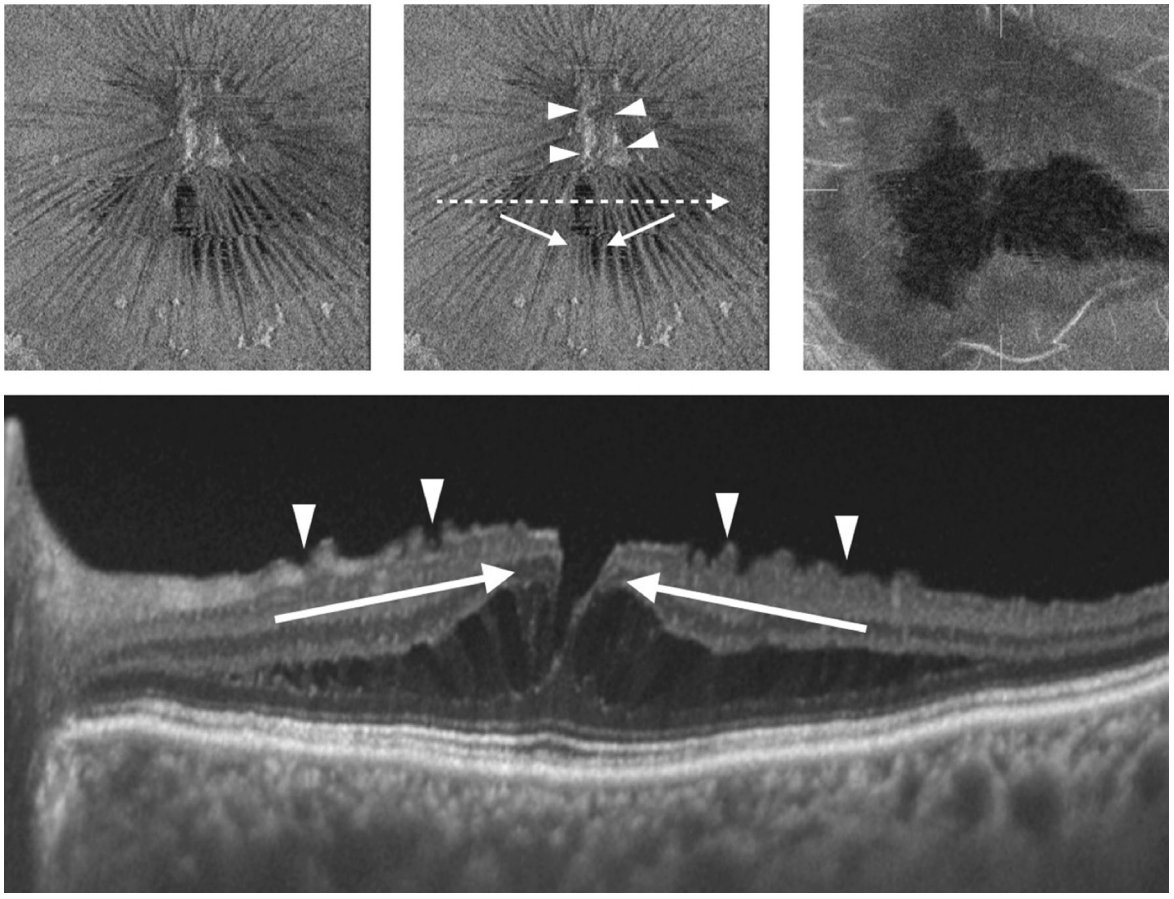

FIGURE 6. Broad schisis-like retinal cleavage in patients with parafoveal epicenter of contractile epiretinal membrane (PEC-ERM) owing to centripetal retinal traction towards the fovea (Group D). (Top left and Top middle) En face images at the level of the internal limiting membrane (ILM) of a representative 88-year-old female patient in Group D. Arrowheads indicate PEC-ERM with surrounding radiating folds. The dotted arrow indicates the location of the B-scan section (Bottom). Solid arrows in the Top middle and Bottom panels indicate the direction of the retinal traction force. The Top right panel shows retinal cleavage at the level of the outer nuclear layer. Arrowheads in the Bottom panel indicate retinal folds.

direction of retinal traction using the circularity of the foveal aperture at the ILM level and at the retinal cleavage area (Supplementary Figure 2 and Figure 5). Generally, when folds are generated in thin elastic membranes, the maximum amplitude of the fold becomes larger as the compression stress on the membrane increases.[26-28] As shown in the top left panel of Figure 5, comparing the 3 groups with retinal folds (Groups B, C, and D) showed that the maximum depth of the deepest fold was significantly greater in Groups C and D compared to Group B, indicating greater retinal traction in tractional LMH compared with MPH. The circularity of the foveal aperture at the ILM level and at the retinal cleavage area were significantly lower in the group with tractional LMH with PEC-ERM (Group D) than in the other groups, indicating heterogeneity of the direction of retinal traction in Group D. We summarize these results in Figure 7. One of the limitations of this investigation was that the material properties of the retina, namely Young's modulus and Poisson's ratio, were assumed to be the same in all patients. Reports have shown that Young's modulus of the ILM increases with age (ie, the elasticity decreases).[29] Although there was no statistically significant difference in the mean ages of all the groups in this study (Table 1), further investigation is needed that takes into account the details of retinal material properties.

Our study revealed that the involvement of retinal traction is smaller in the pathology of degenerative LMH than in either tractional LMH or MPH. This result is in agreement with the results of Gaudric and associates,[19] in which degenerative LMH was observed using en face OCT. These results beg the question: what kind of factors other than retinal traction are involved in the pathology of degenerative LMH? Gaudric and associates[19] and Takahashi and Kishi[30] have suggested that the loss of inner foveal tissue is a key characteristic of degenerative LMH. To date, pathologies reported to generate a loss of inner foveal tissue include aborted formation of a full-thickness macular

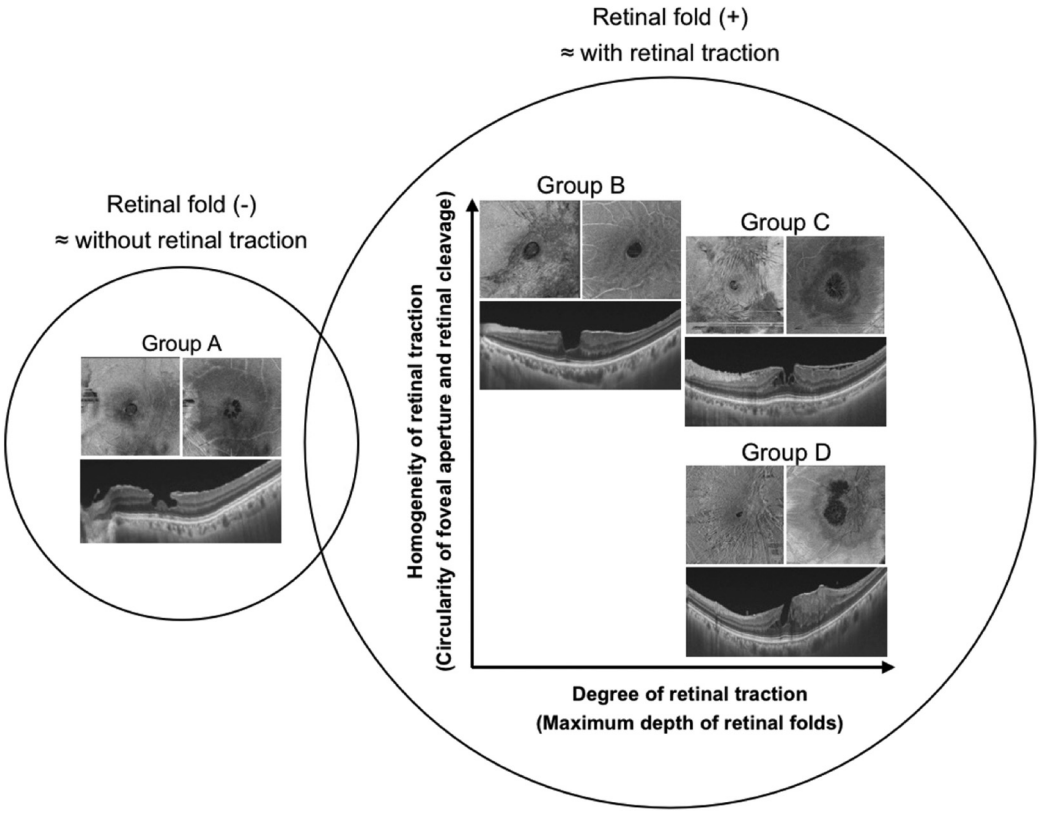

FIGURE 7. Classification of lamellar macular hole (LMH) and macular pseudohole (MPH) based on a multimodal assessment with a combination of en face and B-scan images.

hole,[3,31,32] defect of upper wall in a cystoid macular edema,[1,33,34] and retinoschisis with severe myopia.[14,15] Unfortunately, it is almost impossible to differentiate these background pathologies because it is difficult to observe the entire developmental process of degenerative LMH. Despite this difficulty, visual acuity prognoses and responses to vitreous surgery may differ with differing background pathologies, even if foveal contours in B-scan images do not appear to differ. Further analysis of the developmental process of degenerative LMH with higher resolution of OCT is needed to understand the detailed pathology of degenerative LMH.

Whether LMH and MPH pathologies involve retinal traction has a great influence on treatment strategy. Vitrectomy and ERM/ILM removal may be effective in eliminating pathologic retinal traction in cases of reduced visual acuity and metamorphopsia.[5,6,19] Our results that retinal traction is involved in the pathology of tractional LMH and MPH support this treatment policy. In contrast, indications for surgical treatment of degenerative LMH remain controversial. In agreement with our results (Table 1), degenerative LMH has been reported to be associated with lower visual acuity and a higher prevalence of ellipsoid zone disruption compared with tractional LMH or MPH.[31,35] Therefore, although this condition requires some kind of treatment, vitrectomy and ERM/ILM removal have been reported to be ineffective for the recovery of visual acuity and foveal contour.[36,37] Our observation that there was very little involvement of retinal traction in the pathology of degenerative LMH supports these previous reports. Our results indicate that a sufficient therapeutic effect cannot be expected with vitrectomy and membrane peeling alone, suggesting that treatment with a different approach is essential. This suggests that compensation for the inner foveal tissue defect may be more important in the treatment of degenerative LMH than removal of retinal traction. LHEP is frequently observed in degenerative LMH and is considered to originate from Müller cells or the vitreous[38-40]; thus, we have proposed a surgical technique that compensates for the inner foveal tissue defect by plugging the foveal aperture with LHEP.[41] In our preliminary results, the visual acuity and foveal contour have been significantly improved with this surgical technique.[41] Currently we are investigating long-term postoperative outcomes in a larger number of cases.

There are several important limitations to this study. Firstly, it was retrospective in nature and used a relatively small sample size. Secondly, qualitative analysis of en

face and B-scan images is a subjective evaluation. Finally, the en face imaging resolution is not sufficient to render all the characteristics of LMH and MPH. For example, we were unable to differentiate LHEP and ERM using en face imaging. In summary, we investigated LMH and MPH with a combination of en face and radial B-scan OCT and showed that multimodal OCT assessment enables classification of these diseases based on pathologic conditions, in particular based on the characteristics of retinal traction.

FUNDING/SUPPORT: NO FUNDING OR GRANT SUPPORT. FINANCIAL DISCLOSURES: THE FOLLOWING AUTHORS HAVE NO financial disclosures: Masayuki Hirano, Yuki Morizane, Shuhei Kimura, Mio Hosokawa, Yusuke Shiode, Shinichiro Doi, Shinji Toshima, Kosuke Takahashi, Mika Hosogi, Atsushi Fujiwara, Ippei Takasu, Toshio Okanouchi, Masaya Kawabata, and Fumio Shiraga. The authors attest that they meet the current ICMJE criteria for authorship.

REFERENCES

1. Gass JD. Lamellar macular hole: a complication of cystoid macular edema after cataract extraction: a clinicopathologic case report. *Trans Am Ophthalmol Soc* 1975;73:231–250.
2. Allen AW, Gass JD. Contraction of a perifoveal epiretinal membrane simulating a macular hole. *Am J Ophthalmol* 1976;82(5):684–691.
3. Haouchine B, Massin P, Tadayoni R, Erginay A, Gaudric A. Diagnosis of macular pseudoholes and lamellar macular holes by optical coherence tomography. *Am J Ophthalmol* 2004; 138(5):732–739.
4. Witkin AJ, Ko TH, Fujimoto JG, et al. Redefining lamellar holes and the vitreomacular interface: an ultrahigh-resolution optical coherence tomography study. *Ophthalmology* 2006;113(3):388–397.
5. Hirakawa M, Uemura A, Nakano T, Sakamoto T. Pars plana vitrectomy with gas tamponade for lamellar macular holes. *Am J Ophthalmol* 2005;140(6):1154–1155.
6. Garretson BR, Pollack JS, Ruby AJ, Drenser KA, Williams GA, Sarrafizadeh R. Vitrectomy for a symptomatic lamellar macular hole. *Ophthalmology* 2008;115(5): 884–886.e1.
7. Michalewska Z, Michalewski J, Odrobina D, et al. Surgical treatment of lamellar macular holes. *Graefes Arch Clin Exp Ophthalmol* 2010;248(10):1395–1400.
8. Sun J-P, Chen S-N, Chuang C-C, et al. Surgical treatment of lamellar macular hole secondary to epiretinal membrane. *Graefes Arch Clin Exp Ophthalmol* 2013; 251(12):2681–2688.
9. Duker JS, Kaiser PK, Binder S, et al. The International Vitreomacular Traction Study Group classification of vitreomacular adhesion, traction, and macular hole. *Ophthalmology* 2013; 120(12):2611–2619.
10. Pang CE, Spaide RF, Freund KB. Epiretinal proliferation seen in association with lamellar macular holes: a distinct clinical entity. *Retina* 2014;34(8):1513–1523.
11. dell'Omo R, Virgili G, Rizzo S, et al. Role of lamellar hole-associated epiretinal proliferation in lamellar macular holes. *Am J Ophthalmol* 2017;175:16–29.
12. Govetto A, Dacquay Y, Farajzadeh M, et al. Lamellar macular hole: two distinct clinical entities? *Am J Ophthalmol* 2016; 164:99–109.
13. Zampedri E, Romanelli F, Semeraro F, Parolini B, Frisina R. Spectral-domain optical coherence tomography findings in idiopathic lamellar macular hole. *Graefes Arch Clin Exp Ophthalmol* 2017;255(4):699–707.
14. Rino F, Elena Z, Ivan M, Paolo B, Barbara P, Federica R. Lamellar macular hole in high myopic eyes with posterior staphyloma: morphological and functional characteristics. *Graefes Arch Clin Exp Ophthalmol* 2016;254(11): 2141–2150.
15. Lai T-T, Yang C-M. Lamellar hole-associated epiretinal proliferation in lamellar macular hole and full-thickness macular hole in high myopia. *Retina* 2017; https://doi.org/10.1097/IAE.0000000000001708. [Epub ahead of print].
16. Gupta P, Sadun AA, Sebag J. Multifocal retinal contraction in macular pucker analyzed by combined optical coherence tomography/scanning laser ophthalmoscopy. *Retina* 2008; 28(3):447–452.
17. Tammewar AM, Bartsch D-U, Kozak I, et al. Imaging vitreomacular interface abnormalities in the coronal plane by simultaneous combined scanning laser and optical coherence tomography. *Br J Ophthalmol* 2009;93(3):366–372.
18. Fujiwara A, Morizane Y, Hosokawa M, et al. Factors affecting choroidal vascular density in normal eyes: quantification using en face swept-source optical coherence tomography. *Am J Ophthalmol* 2016;170:1–9.
19. Gaudric A, Aloulou Y, Tadayoni R, Massin P. Macular pseudoholes with lamellar cleavage of their edge remain pseudoholes. *Am J Ophthalmol* 2013;155(4):733–742.e1-4.
20. Clamp MF, Wilkes G, Leis LS, et al. En face spectral domain optical coherence tomography analysis of lamellar macular holes. *Retina* 2014;34(7):1360–1366.
21. Olsen E. Particle shape factors and their use in image analysis-Part I: Theory. *Journal of GxP Compliance* 2011;15(7):85–96.
22. Michalewski J, Michalewska Z, Dzięgielewski K, Nawrocki J. Evolution from macular pseudohole to lamellar macular hole - spectral domain OCT study. *Graefes Arch Clin Exp Ophthalmol* 2011;249(2):175–178.
23. Wagner H. Flat sheet metal girders with very thin metal web. Part I: general theories and assumptions. *NACA Technical Memorandum 604* 1931;20(8):200–207.
24. Akita T, Nakashino K, Natori MC, Park KC. A simple computer implementation of membrane wrinkle behavior via a projection technique. *Int J Numer Meth Eng* 2007;71(10): 1231–1259.
25. Compera D, Schumann RG, Cereda MG, et al. Progression of lamellar hole-associated epiretinal proliferation and retinal changes during long-term follow-up. *Br J Ophthalmol* 2018; 102(1):84–90.
26. Miyazaki Y. Wrinkle/slack model and finite element dynamics of membrane. *Int J Numer Meth Eng* 2006;66(7): 1179–1209.

27. Roddeman DG, Drukker J, Oomens CWJ, Janssen JD. The wrinkling of thin membranes: Part I-Theory. *J Appl Mech* 1987;54(4):884–887.
28. Roddeman DG, Drukker J, Oomens CWJ, Janssen JD. The wrinkling of thin membranes: Part II-Numerical analysis. *J Appl Mech* 1987;54:888–892.
29. Candiello J, Cole GJ, Halfter W. Age-dependent changes in the structure, composition and biophysical properties of a human basement membrane. *Matrix Biol* 2010;29(5):402–410.
30. Takahashi H, Kishi S. Tomographic features of a lamellar macular hole formation and a lamellar hole that progressed to a full-thickness macular hole. *Am J Ophthalmol* 2000; 130(5):677–679.
31. Bottoni F, Deiro AP, Giani A, Orini C, Cigada M, Staurenghi G. The natural history of lamellar macular holes: a spectral domain optical coherence tomography study. *Graefes Arch Clin Exp Ophthalmol* 2013;251(2):467–475.
32. Bottoni F, Carmassi L, Cigada M, Moschini S, Bergamini F. Diagnosis of macular pseudoholes and lamellar macular holes: is optical coherence tomography the "gold standard"? *Br J Ophthalmol* 2008;92(5):635–639.
33. Unoki N, Nishijima K, Kita M, et al. Lamellar macular hole formation in patients with diabetic cystoid macular edema. *Retina* 2009;29(8):1128–1133.
34. Tsukada K, Tsujikawa A, Murakami T, Ogino K, Yoshimura N. Lamellar macular hole formation in chronic cystoid macular edema associated with retinal vein occlusion. *Jpn J Ophthalmol* 2011;55(5):506–513.
35. Pang CE, Spaide RF, Freund KB. Comparing functional and morphologic characteristics of lamellar macular holes with and without lamellar hole-associated epiretinal proliferation. *Retina* 2015;35(4):720–726.
36. Schumann RG, Compera D, Schaumberger MM, et al. Epiretinal membrane characteristics correlate with photoreceptor layer defects in lamellar macular holes and macular pseudoholes. *Retina* 2015;35(4): 727–735.
37. Choi WS, Merlau DJ, Chang S. Vitrectomy for macular disorders associated with lamellar macular hole epiretinal proliferation. *Retina* 2017; https://doi.org/10.1097/IAE.0000000000001591. [Epub ahead of print].
38. Parolini B, Schumann RG, Cereda MG, Haritoglou C, Pertile G. Lamellar macular hole: a clinicopathologic correlation of surgically excised epiretinal membranes. *Invest Ophthalmol Vis Sci* 2011;52(12):9074–9083.
39. Compera D, Entchev E, Haritoglou C, et al. Lamellar hole-associated epiretinal proliferation in comparison to epiretinal membranes of macular pseudoholes. *Am J Ophthalmol* 2015; 160(2):373–384.e1.
40. Pang CE, Maberley DA, Freund KB, et al. Lamellar hole-associated epiretinal proliferation: a clinicopathologic correlation. *Retina* 2016;36(7):1408–1412.
41. Shiraga F, Takasu I, Fukuda K, et al. Modified vitreous surgery for symptomatic lamellar macular hole with epiretinal membrane containing macular pigment. *Retina* 2013;33(6): 1263–1269.